

# Plasma density evolution during nanosecond discharge in hydrogen gas at $(1-3) \times 10^5$ Pa pressure

S Yatom and Ya E Krasik

Department of Physics, Technion, Haifa 32000, Israel

E-mail: [shurik@physics.technion.ac.il](mailto:shurik@physics.technion.ac.il) and [fnkrasik@physics.technion.ac.il](mailto:fnkrasik@physics.technion.ac.il)

Received 9 January 2014, revised 31 March 2014

Accepted for publication 10 April 2014

Published 7 May 2014

## Abstract

The results of a study of the nanosecond discharge in H<sub>2</sub> gas at pressures of  $(1-3) \times 10^5$  Pa using fast-framing photography and space- and time-resolved spectroscopy are presented. The discharge is initiated by the application of a high-voltage pulse with an amplitude of  $\sim 100$  kV and duration of  $\sim 5$  ns to a blade cathode placed at a distance of 20 mm from the anode. The results show the dynamics of the discharge formation and the build-up of the plasma electron density in the discharge channels close to and at a distance from the edge of the cathode. The results obtained are compared to those obtained in recent studies of similar discharges in air and He gas. It was shown that the time and space evolution of the plasma light emission in the H<sub>2</sub> gas discharge is very similar to that in air. Namely, the generation of the plasma is mainly confined to the plasma channels initiated at the top and bottom edges of the cathode electrode and that there are no new plasma channels formed from the explosive emission centres along the blade as it was obtained in earlier experiments with He gas. Spectroscopic measurements showed that the plasma density reaches  $2 \times 10^{17}$  cm<sup>-3</sup> and  $1.6 \times 10^{16}$  cm<sup>-3</sup> in the vicinity of the cathode and the middle of the anode-cathode gap, respectively, for a plasma electron temperature of  $< 1.5$  eV. The values of plasma electron density and the previously presented results of electric field measurements allow calculation of the resistance of the plasma channels.

Keywords: nanosecond discharge, plasma resistivity, optical emission spectroscopy, runaway discharge, gas discharge diagnostics

(Some figures may appear in colour only in the online journal)

## 1. Introduction

Nanosecond (ns) timescale electrical discharges in pressurized ( $P \geq 10^5$  Pa) gases have been widely investigated in recent years using optical diagnostics [1–3] in order to understand the phenomena governing this type of discharge. The plasma produced in such discharge is employed in pumping pulsed lasers [4], energy release in microwave compressors [5], switches for low-inductance, high-current gas spark gaps [6] and fast combustion of gas mixtures [7], and has promising potential for application in biomedical treatments [8]. The results of this research, carried out with different gases and pressures [9, 10] in repetitive and single pulse application modes [3, 11–15] share some similar features, for instance a diffuse-like structure, fast light emission front propagation

from cathode to anode, the generation of runaway electrons, etc. The main experimental difficulty in this research is due to the fact that the development of the discharge occurs in the nano- and sub-ns timescale, which requires the application of non-disturbing diagnostic methods with this scale of time resolution. A major part of the experimental results obtained so far concerns the time-integrated light emission from the discharge plasma channel, rather than the time-resolved dynamics of the parameters of plasma channel formation. One of the main conclusions of this research is that the first stage of the discharge is characterized by the formation of the plasma channels from the explosive emission centres on the cathode's edge, which advance towards the anode with a velocity  $\sim 10^8$ – $10^9$  cm s<sup>-1</sup> [16]. It was shown that when light-emitting plasma channels approach the anode, the gap is not

short-circuited and the plasma generation continues [17, 18]. In addition, it was found that the increase in the pressure of the gas leads to a decrease in the diffusivity of the plasma channels, which acquire a contracted form. Recent studies, where fast-framing photography was used, showed the dynamics of the light emission of the discharge in air [17, 18] and He gas [19]. The results of time-integrated studies of the plasma electron density in the case of repetitive discharge was reported in [20] and with a time resolution  $<1$  ns in a single discharge in He gas at  $P = 10^5$  Pa in [21]. It was also shown that after the initial bridging of the cathode–anode (C–A) gap by the plasma channels, the subsequent development of the discharge in He and air is essentially different [19].

In this paper, we present the results of a time- and space-resolved study of the discharge light emission and density evolution in  $H_2$  gas at  $P = 10^5$ ,  $2 \times 10^5$  and  $3 \times 10^5$  Pa, using fast-framing photography and visible spectroscopy. The choice of  $H_2$  as an experimental gas was due to two main reasons. First of all,  $H_2$  was widely used in experiments but plasma parameters in  $H_2$  were not studied with optical emission spectroscopy (OES), especially not in single pulse mode and not with temporal resolution of single ns. In addition we recently have measured the electric field in plasma channels in  $H_2$  discharge using coherent anti-Stokes Raman scattering (CARS [22]). Data on plasma electron density can be used together with the data on electric field to evaluate the plasma resistivity. Also we have carried out a fast-framing photography experiment both to compare the dynamics of the plasma channels in  $H_2$  to those in air and He and to easily understand the spectroscopic results, knowing the channel structure. The results are compared to those obtained in different gases under very similar conditions [17–19, 21].

## 2. Experimental setup

The discharge in  $H_2$  gas was initiated by a high-voltage (HV) pulse with an amplitude of  $\sim 100$  kV and duration of 5 ns at a full-width at half-maximum (FWHM) generated by a pulse ns-generator [17]. The output of the ns-generator is connected to the oil-filled transmission coaxial line which transfers the HV pulse through the interface insulator to the gas-filled experimental chamber. The wave impedance of the coaxial line  $Z = 60\epsilon^{-1/2}\ln(R/r)$ , where  $\epsilon$  is the dielectric constant of the transformer oil and  $R$  and  $r$  are the inner radii of the external and internal tubes of the coaxial line, was  $100 \Omega$  in order to match the generator's output impedance. At the output of this transmission line a homemade calibrated B-dot and capacitive voltage divider (VD) were placed (see figure 1) to measure the current and voltage waveforms, respectively. The current and waveforms from the VD and B-dot loop were acquired using a TDS 694C oscilloscope ( $3$  GHz,  $10$  Gs  $s^{-1}$ ) (see figure 2).

The output of the transmission line was connected to the cathode holder via the interface insulator of the experimental chamber. Prior to the experiments, the discharge chamber was pumped to  $P \approx 10$  Pa and then filled with  $H_2$  gas at pressures  $P = 10^5$ ,  $2 \times 10^5$  and  $3 \times 10^5$  Pa. The chamber has two perspex windows for observation of light emission. The HV pulse is applied to a cathode made of a stainless steel shaving blade.

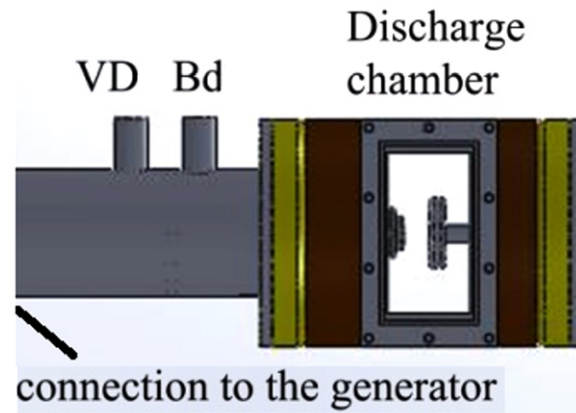


**Figure 1.** Discharge chamber and the measurement configuration; VD: voltage divider, Bd: B-dot sensor.

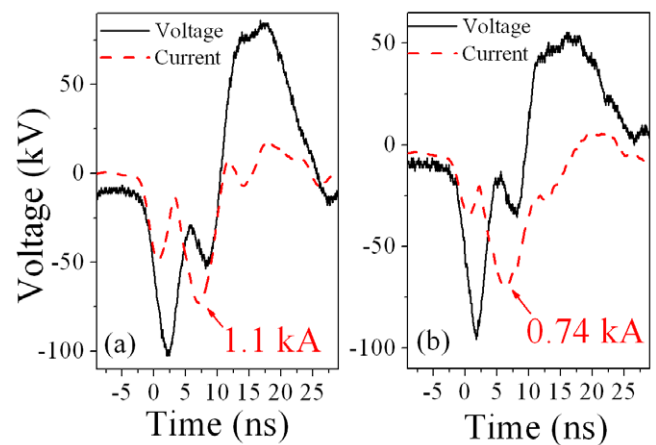


**Figure 2.** Voltage and current waveforms: (a)  $d_{CA} = 20$  mm,  $P = 3 \times 10^5$  Pa; (b)  $d_{CA} = 20$  mm,  $P = 2 \times 10^5$  Pa.

The blade has a sharp edge, about  $5 \mu\text{m}$  thick, ensuring electric field enhancement near the cathode edge. The blade has a length of 7 mm, so that depleted explosive plasma emission centres on the blade edge are replaced by neighbouring ones. In order to avoid emission from the cathode holder, a special screen cover made of Teflon was used. The anode was made of a 150 mm diameter aluminum disc and the C–A gap  $d_{CA}$  can be regulated in the range 0–4 cm but in the majority of experiments the C–A gap was set to  $d_{CA} = 20$  mm.

In experiments with fast-framing photography, the light emission from the discharge plasma was recorded using a fast intensified 4QuikE camera in the spectral range 350–700 nm (see figure 3(a)). In the spectroscopy experiments (see figure 3(b)), the light emission from the gas discharge plasma was observed through a perspex window and focused on the entrance slit ( $100 \mu\text{m}$  in width and 20 mm in height) of a Chromex-500 imaging spectrometer with a lens. The latter was placed at an appropriate focal length for the  $H_\alpha$  spectral line wavelength. The instrumental broadening and the dispersion for the  $H_\alpha$  spectral line were determined using a hydrogen calibration lamp, and were  $0.6 \text{ \AA}$  and  $0.12 \text{ \AA}/\text{pixel}$ , respectively. The CCD matrix of the camera had  $300 \times 780$  elements, with the longer horizontal axis corresponding to the dispersion direction. The synchro-pulse of the 4QuikE

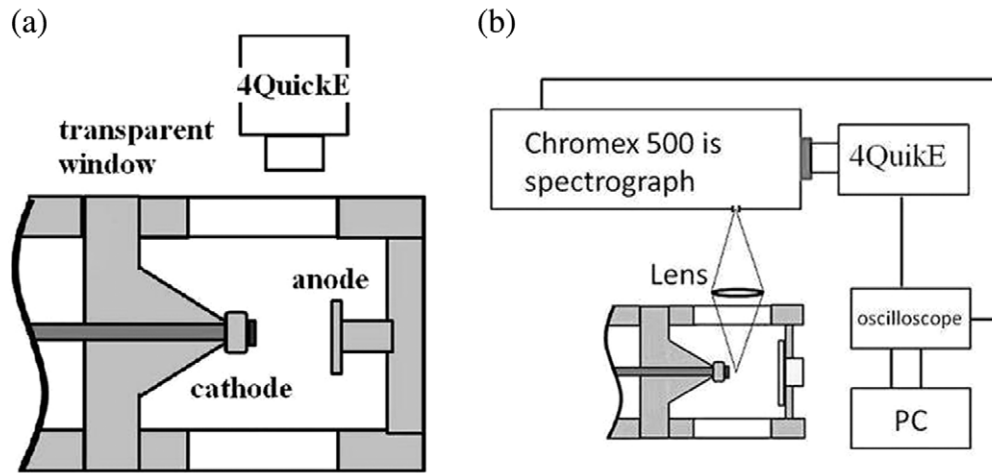


**Figure 3.** Experimental setup. (a) Setup for fast-framing photography; (b) setup for spectroscopic measurements.

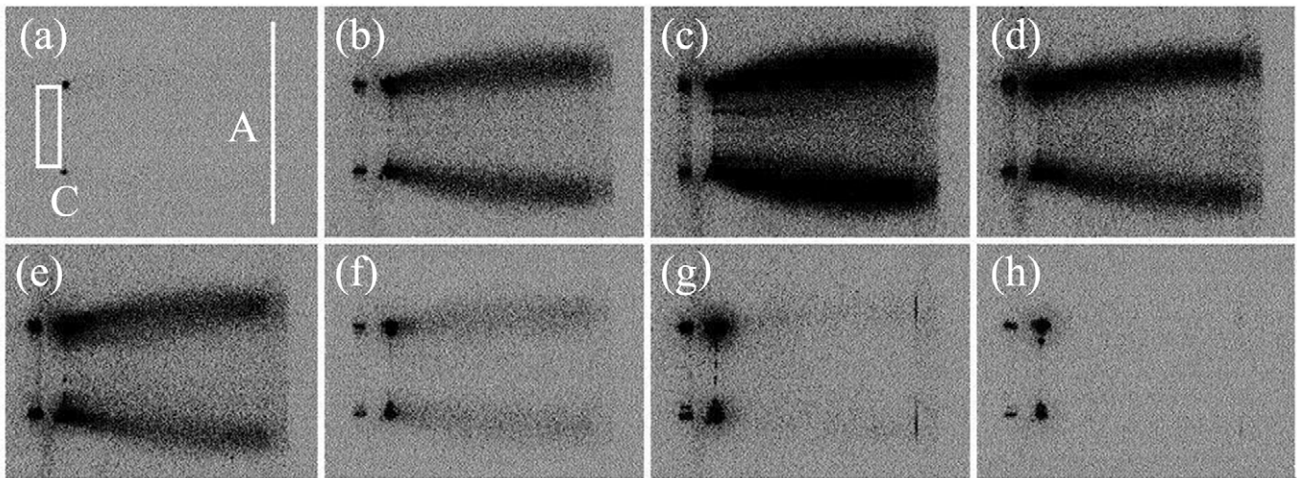


**Figure 4.** Development of the discharge at  $P = 2 \times 10^5$  Pa. (a) Onset of light emission at the cathodes' edges ( $t \approx 0.1$  ns); (b), (c) plasma channels bridge the C–A gap and dense light emission front spreads through the established channel (1–5 ns); (d), (e) dense light emission at the front recedes back from cathode to anode; (f), (h) evanescence of plasma from the C–A gap volume until the light is emitted from only the spots at the top and bottom cathode edges (8–14 ns). All times are given with respect to the onset of light emission from the cathode edges.

camera was acquired by the same TDS 694C oscilloscope together with voltage and current waveforms, and the image of the spectral line was recorded via 4QuikE camera software. This allowed us to assign each image its time with respect to the appearance of the first distinct spectral line shape. The lens–spectrometer–4QuikE camera system was mounted on a single base, which was moved using a micrometer to allow observation of different locations in the C–A gap. In the experiments, light emission from the plasma was collected from the vicinity of the blade–cathode edge and from the middle of the C–A gap. In fact, because of the divergence of light rays passing through the lens, the light emission from the plasma was actually collected from the locations  $d_C = 0$ –2 mm and  $d_C = 4$ –6 mm, with respect to the edge of the cathode along the C–A axis and a few mm above and beyond it, corresponding to  $d_C = 1$  mm and  $d_C = 5$  mm, respectively.

To trigger the 4QuikE camera (frame duration of 2 ns) a synchro-pulse from the first compression stage of the pulse

generator was used. The time jitter of this trigger allowed the observation of different stages of the discharge in different shots. Each generator shot was assigned its time with respect to  $t = 0$  when the voltage reaches  $\sim 30\%$  of its amplitude, and one obtains the beginning of the light emission. On average,  $\sim 100$  shots were recorded for experiments at  $H_2$  gas pressures  $P = 10^5$ ,  $2 \times 10^5$  and  $3 \times 10^5$  Pa, for each position ( $d_C = 1$  mm and  $d_C = 5$  mm).

### 3. Experimental results and data processing

The sequences of frames representing the development of the discharge light emission at  $P = 2 \times 10^5$  and  $3 \times 10^5$  Pa are shown in figures 4 and 5. The results are very similar to those reported in [12, 13] for discharges in air. Namely, one can see that the discharge channels originate at the top and bottom edges of the cathode where the largest enhancement of the electric field is realized. These discharge channels propagate

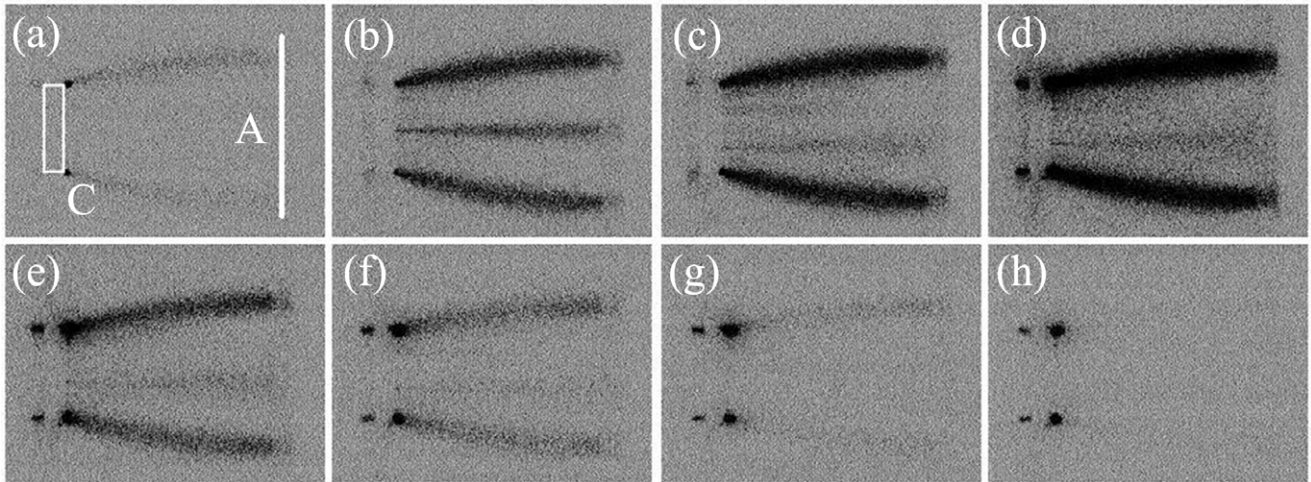


**Figure 5.** Development of the discharge at  $P = 3 \times 10^5$  Pa. (a) Plasma streamers bridge the C–A gap ( $t \sim 0.6$  ns); (b)–(d) the intensity of light emission grows throughout the established plasma channel (1–3 ns); (e)–(g) plasma channel decay (4–7 ns); (h) evanescence of plasma from the C–A gap volume until the light is emitted from only the spots at the top and bottom cathode edges (8–10 ns). All times are given with respect to the onset of light emission from the cathode edges.

towards the anode but do not terminate the HV pulse once they bridge the C–A gap, as would have been expected in the case of low-resistive plasma. The subsequent development of the discharge is the build-up of the plasma in these established channels characterized by a gradual increase in light emission. The front of this enhanced light emission also propagates from the cathode to anode. During the last stage of the discharge, one can see that the light emission decreases first at the anode side, finally leaving the edges of the cathode as the only light emission sources. In the case of increased pressure,  $P = 3 \times 10^5$  Pa, the discharge channels become contracted in much the same way as in experiments in air [17]. Thus, the dynamics of light emission from the plasma formed during the discharge in  $H_2$  gas is similar to that in air, unlike the discharge in He gas, where the later stages of the discharge are governed by the formation of explosive emission centres at the edge of the cathode [19].

In general, a common method to determine the density of hydrogen plasma is the measurement and analysis of the FWHM of  $H_\alpha$  and  $H_\beta$  spectral lines. However, in the case of a relatively dense ( $\sim 10^{16} \text{ cm}^{-3}$ ) plasma generated in rather low-ionized hydrogen gas, the  $H_\beta$  spectral line becomes almost unresolvable because of significant Stark broadening and the  $H_2$  molecular spectrum, which has strong bands in this spectral range. In this case the plasma electron density ( $n_e$ ) can be obtained by the measurement and analysis of the  $H_\alpha$  spectral line using tabulated data [23] for Stark broadening that include the ion dynamics. However, for low-ionized plasma produced in a discharge at large gas pressure, one has also to consider the resonance and van der Waals (VdW) broadening mechanisms. In weakly ionized and cold plasma, the majority of H atoms are in the ground state [21], which is a singlet s state. Consequently, transitions from or to a singlet p level are affected by resonance broadening, which can be estimated as [21]

$$2\omega_i^r \approx 9 \times 10^{-14} N_g \sqrt{\frac{g_g}{g_i} \frac{f_{gi}}{E_{ig}}}, \quad (1)$$

where  $N_g$  ( $\text{cm}^{-3}$ ) is the density of H atoms,  $g_g$  and  $g_i$  are the degeneracies of the ground and either the initial or final energy level connected to the ground state by a dipole-allowed transition with absorption strength  $f_{gi}$  and energy  $E_{ig}$  ( $\text{cm}^{-1}$ ). For  $N_g \approx 2 \times 10^{19} \text{ cm}^{-3}$ , one obtains  $2\omega_i^r \approx 2.6777 \text{ cm}^{-1} = 0.1152 \text{ nm}$ . In addition, following [21], the VdW broadening can be estimated (in atomic units ( $m_e = e = \hbar = 1$ )) as

$$2\omega_{if}^{\text{VdW}} = 2 \times 10^{-16} N_g \left( \frac{T_n}{\mu} \right)^{3/10} \frac{(\overline{R_i^2} - \overline{R_f^2})^{2/5}}{E_p^{4/5}}, \quad (2)$$

where  $T_n$  (eV) is the neutrals' temperature,  $\mu$  is the reduced mass,  $E_p$  ( $\text{cm}^{-1}$ ) is the excitation energy of the upper level, and  $R_i$  and  $R_f$  are the radii vectors of the radiator in states  $i$  and  $f$ , respectively, in the units of the Bohr radius. For low-ionized plasma, the value of  $\overline{R^2}$  can be estimated as [24]

$$\overline{R^2} = \frac{n_*^2}{2} [5n_*^2 + 1 - 3l(l+1)], \quad (3)$$

where  $n_*$  is the effective principal quantum number, given by  $1/\sqrt{2I_l}$ , with  $I_l$  being the ionization energy of state  $l$ , and  $l$  its orbital momentum. For  $N_g \approx 2 \times 10^{19} \text{ cm}^{-3}$ , one has  $2\omega_{if}^{\text{VdW}} \approx 0.5113 \text{ cm}^{-1} = 0.044 \text{ nm}$ . In the present research, the electron temperature  $T_e$  was not measured; however, estimations [21] show that the value of  $T_e$  is  $\leq 2$  eV. Using the interpolating plots of the FWHM of the  $H_\alpha$  spectral line versus  $n_e$  for  $T_e = 5000, 10000, 15000$  and  $20000$  K, the value of  $n_e$  was calculated for the measured values of the FWHM of the  $H_\alpha$  spectral line, including the VdW and resonance broadening effects. The  $H_\alpha$  spectral line intensity profiles at different time of the discharge obtained from the plasma at  $d_C = 5$  mm and  $d_C = 1$  mm are shown in figures 6(a) and (b). In a comparison of the FWHM and intensity of  $H_\alpha$  (figures 6(a) and (b)) obtained at these two positions, one can see that at  $d_C = 1$  the FWHM is larger and the intensity is smaller than the FWHM and intensity of  $H_\alpha$  at  $d_C = 5$  mm. Here let us note that the intensity of the

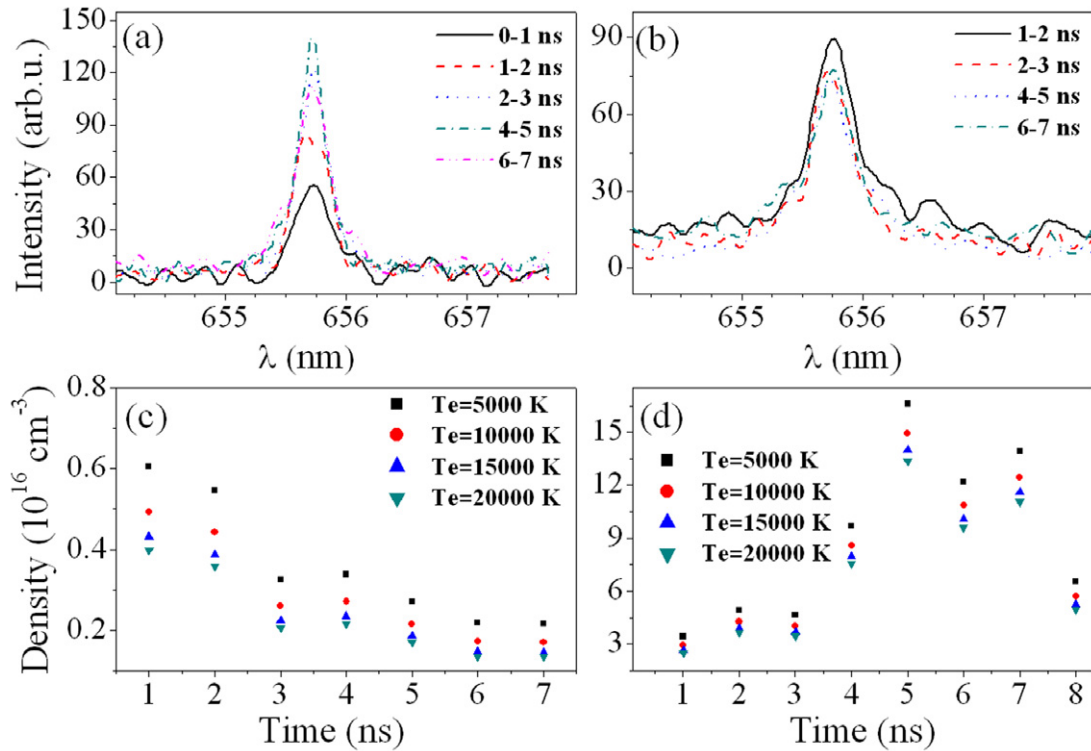


**Figure 6.** Temporal evolution of  $H_\alpha$  Balmer lines at pressure  $P = 10^5$  Pa. Evolution of  $H_\alpha$  spectral line at (a)  $d_C = 5$  mm and (b)  $d_C = 1$  mm and densities calculated from the Stark broadening of  $H_\alpha$  line at (c)  $d_C = 5$  mm and (d)  $d_C = 1$  mm. For the sake of clarity of the plots, curves representing some time intervals were omitted in the figure.

spectrally-integrated light emission near the cathode is higher on average than that in the middle of the channel (see figures 4 and 5). The evaluations of the line-centre optical thickness of the  $H_\alpha$  line, assuming the temperature of the neutrals to be  $\sim 0.03$  eV [21], and the electron temperature  $T_e < 2$  eV yields  $\tau < 1$ , hence implying that the line shape and its width are not significantly affected by self-absorption.

The temporal evolution of  $n_e$  is shown in figures 6(c) and (d) for  $d_C = 1$  and 5 mm. We have collected  $\sim 100$  shots for the  $H_\alpha$  lines at each position and each pressure. All these shots belong to the time interval 0–9 ns, with respect to the onset of light emission from the plasma. The shots were divided into groups belonging to the 1 ns interval. In this way, for instance, the spectral line representing the time interval of 0–1 ns is an average spectral line of  $\sim 10$  single shots taken at times between 0 and 1 ns with respect to the onset of the light emission. The standard errors bars, stemming from the system resolution were not shown in the presented plots in order to keep the plot readable. The errors were largest for the lowest FWHM values where they reached up to 24%. The smallest errors were  $\sim 11\%$ . One can see that there is a substantially different dynamics of the plasma density evolution for these two locations. At  $d_C = 1$  mm, the density is significantly higher than at  $d_C = 5$  mm, and it grows in time, reaching its peak of  $< 1.6 \times 10^{17} \text{ cm}^{-3}$  in a few ns, and then the plasma density decays. At  $d_C = 5$  mm, the maximum  $n_e$  of  $< 6 \times 10^{15} \text{ cm}^{-3}$  is obtained earlier in the pulse with a following gradual decrease to 2/3 of its initial maximal value. Let us note here that the error introduced by neglecting the VdW and resonance widths would be very significant. Indeed,

the VdW and resonance broadening contribute 0.044 nm and 0.1152 nm, respectively. Thus, with the FWHM values of the  $H_\alpha$  line ranging from 0.24 to 1.6 nm (for different time intervals and observation locations) the error introduced by neglecting the VdW and resonance widths reaches as high as almost 50% in the middle of the plasma channel, where the line widths show the lowest values.

#### 4. Discussion

To summarize, fast-framing photography showed that light-emitting plasma exists in the C–A gap for  $\sim 10$  ns at  $P = 10^5$  Pa and  $\sim 8$  ns at  $P = 2 \times 10^5$  and  $3 \times 10^5$  Pa. Bright spots at the cathode’s edge, which serve as the origin for the discharge channels, remain for  $\sim 18$  ns after the appearance of the light emission. Visually, the discharge in  $H_2$  gas is very similar to that in air [17], except for the velocity of the initial plasma light emitting front propagation from the cathode towards the anode and the fact that in air the channels appear contracted at a pressure  $P = 2 \times 10^5$  Pa and in  $H_2$  that happens at  $P = 3 \times 10^5$  Pa. Although the time resolution of the present experimental setup did not allow us to calculate the precise velocity of the light front propagation, nevertheless it was obvious that, at least in the first stage of the discharge, this velocity is  $< 2$  times higher than those measured for discharges in He and air [17, 19]. The generation of the plasma is confined mainly to the top and bottom channels during the whole discharge, and there are no new plasma channels formed from the explosive emission centres along the blade as obtained

in the case of He gas. This difference between He and both H<sub>2</sub> and air can be related to the almost two times higher molar ionization energies for He than for H<sub>2</sub> and N<sub>2</sub> gases.

Measurements of the plasma electron density at  $P = 10^5$  Pa showed different evolutions of plasma near the cathode and in the middle of the C–A gap. The plasma density at the bright spots, which serve as origins for the main discharge channels bridging the C–A gap, is significantly higher than that measured in the middle of the channel. The density at these cathode spots grows in time for  $<5$  ns to values of 5 times the initial value, before showing decay. At the channel's middle, the plasma density evolution is quite different, with the largest values being measured in the first nanosecond and the subsequent decay to approximately 2/3 of the initial value. The decrease in the density can be related to the spreading of the channel in the direction perpendicular to that of the C–A axis and to the decrease in the plasma electron temperature due to formation of the plasma, which decreases the mean free path of electrons. The highest measured value of  $n_e$  at  $d_C = 1$  mm is  $<25$  times higher than the highest value of  $n_e$  at  $d_C = 5$  mm, and the lowest value of  $n_e$  at  $d_C = 1$  mm is approximately thrice the highest value of  $n_e$  at  $d_C = 5$  mm. This difference in the plasma density between the two regions is very pronounced as opposed to the results reported for the discharge in He gas [21]. However, one can relate the larger and growing electron density at the cathode edges in H<sub>2</sub> gas to the fact that the discharges develop only along those channels, while in He gas the discharge channels are formed and decay also at other locations of the cathode on a time scale of  $\sim 2$  ns.

Using the density measurements presented in this work together with the data on electric field from [22] one can estimate the resistivity of plasma. The conductivity of the low-ionized gas can be estimated as [25]

$$\sigma [\Omega^{-1} \text{cm}^{-1}] = 2.82 \times 10^{-4} \frac{n_e [\text{cm}^{-3}]}{v_m [\text{s}^{-1}]}. \quad (4)$$

Here  $v_m = n_n V_e \sigma_{tr} + n_e V_e \sigma_c$  is the total collisional electron frequency with neutrals and ions, where  $\sigma_c = 2.87 \times 10^{-14} (T_e [\text{eV}])^{-2} \ln \Lambda \approx 7 \times 10^{-14} \text{cm}^2$  is the Coulomb collisional cross-section for plasma electron temperature  $T_e \approx 1\text{--}2$  eV and  $\sigma_{tr}$  is the transport collisional frequency of the plasma electrons with neutrals which is the range  $\sigma_{tr} = 10^{-15}\text{--}10^{-16} \text{cm}^2$ . One can see that for the density of neutrals  $n_n \approx 2 \times 10^{19} \text{cm}^{-3}$  and plasma density  $n_e \leq 10^{16} \text{cm}^{-3}$  the dominant collision process for electrons is the collisions with neutrals even for  $\sigma_{tr} = 10^{-16} \text{cm}^2$ .

Thus, one can estimate the collision frequency of electrons as  $v_m \approx n_n V_e \sigma_{tr} \approx 3 \times 10^{12} \text{s}^{-1}$  for the average thermal velocity of the plasma electrons  $\overline{V_e} = 6.7 \sqrt{T [\text{eV}]} \approx 10^8 \text{cm s}^{-1}$ ,  $n_n \approx 2 \times 10^{19} \text{cm}^{-3}$  and  $\sigma_{tr} = 5 \times 10^{-16} \text{cm}^2$ . These rough estimates showed that the value of the conductivity could be  $\sigma \approx 0.5 \Omega^{-1} \text{cm}^{-1}$  resulting in a current density  $j = \sigma E$  up to  $15 \text{kA cm}^{-2}$  which can be realized in the plasma in the case of electric field  $E \approx 30 \text{kV cm}^{-1}$ .

In experiments, the maximal amplitude of the discharge current was  $I \leq 0.8 \text{kA}$  at  $t \approx 2.5$  ns when the electric field inside the gap, depending on the gas pressure, was in the range  $10\text{--}30 \text{kV cm}^{-1}$ . Framing side and front view images

(front view images were not shown in the manuscript but obtained in the experiments) allow one to estimate the cross-section area of the brightest plasma channels originated from the top and bottom edges of the cathode blade. This rough estimate gives  $S \approx 4 \text{mm}^2$  (for each channel) resulting in a current density through each channel of  $j \approx 10 \text{kA cm}^{-2}$  and, respectively, plasma conductivity in the range  $0.3\text{--}1 \Omega^{-1} \text{cm}^{-1}$ . Taking into account the uncertainty in the determination of the discharge channel cross-sectional area and in fact, unknown radial plasma density distribution, this estimate of the plasma conductivity agrees satisfactory with the estimates described above. Now, one can roughly estimate the average resistance of two plasma channels as  $R_{ch} = \sigma^{-1} l S^{-2} \approx 75 \Omega$  for the effective length of the plasma channel  $l \approx 3$  cm and  $\sigma \approx 0.5 \Omega^{-1} \text{cm}^{-1}$ . This estimated resistance agrees with the value of average resistance obtained from the waveforms of the discharge current and calculated resistive voltage across the cathode anode gap. It is understood that such high resistance results in a large Ohmic energy deposition into the discharge channels which could be in our case up to  $<0.25$  J. The latter gives the averaged temperature of neutrals in the discharge channel as up to  $<150^\circ\text{C}$  with a corresponding sharp increase in the pressure  $<6$  times and, respectively, the generation of shock waves. Here let us note that these calculations of the conductivity can be considered only as rough estimation the order of the magnitude of the resistance of these channels. Taking into account the errors in the estimations of the channel length, its cross-section and the conductivity, the error in the calculated resistance of the plasma channel can be up to 40%.

## 5. Conclusions

The nanosecond discharge in H<sub>2</sub> gas at pressures  $(1\text{--}3) \times 10^5$  Pa was investigated using optical emission spectroscopy. The structure of the discharge is documented with fast-framing imaging, in order to understand the corresponding data obtained using spectroscopy diagnostics. It was shown that the discharge in H<sub>2</sub> gas is similar to that observed in air. Namely the main discharge channels are formed on the top and bottom edges of the cathode and they remain there for the whole discharge duration, as opposed to the discharge in He gas. The difference between the dynamics of the discharge is attributed to the molecular ionization energy, which is almost twice as high in He, as compared with the molecular ionization energy of N<sub>2</sub> and H<sub>2</sub> gases. Also the observed evolution of electron density near and away from the cathode is owed to the channel structure. It was found that near the cathode the plasma density values are higher and grow significantly in time. This is due to a large current density which is realized in those locations because of a narrow part of the channels' origin. In the middle of the C–A gap the channel is much more diffusive; its cross-section is much larger, resulting in a lower current density. After the C–A gap is crossed by the plasma channel in the first nanosecond the plasma electron density in the channel has reached its maximum, and its value gradually decays to 1/3 of its peak. Additionally, the measured plasma electron density together with the electric fields reported in [22] are

employed for calculations of the plasma resistivity. Rough calculations yield a value of  $\sigma \approx 0.5 \Omega^{-1} \text{cm}^{-1}$  for the plasma conductivity resulting in a total resistance of tens of ohms for a plasma channel with an effective length of several centimetres.

## References

- [1] Alekseev S B, Gubanov V P, Kostyrya I D, Orlovskii V M, Skakun V S and Tarasenko V F 2004 *Quantum Electron.* **34** 1007
- [2] Tarasenko V F, Skakun V S, Kostyrya I D, Alekseev S B and Orlovskii V M 2004 *Laser Part. Beams* **22** 75
- [3] Tarasenko V F, Tel'minov A E and Burachenko A G 2011 *Tech. Phys. Lett.* **37** 267
- [4] McDaniel E W and Nighan W L 1982 *Gas Lasers* (New York: Academic)
- [5] Bix D L and Scalapino D J 1980 *J. Appl. Phys.* **51** 3629
- [6] Martin J C 1996 *On Pulsed Power* (New York: Plenum)
- [7] Starikovskii A Y, Anikin N B, Kosarev I N, Mintoussov E I, Nudnova N N, Rakitin A E, Roupasov D V, Starikovskaia S M and Zhukov V P 2008 *J. Propulsion Power* **24** 1182
- [8] Maltsev A N 2006 *IEEE Trans. Plasma Sci.* **34** 1166
- [9] Kostyrya I D, Skakun V S, Tarasenko V F, Tkachev A N and Yakovlenko S I 2004 *Lett. JTF* **30** 31 (in Russian)
- [10] Tarasenko V F and Yakovlenko S I 2005 *Plasma Dev. Oper.* **13** 231
- [11] Shao T, Zhang C, Niu Z, Yan P, Tarasenko V F, Baksht E Kh, Burachenko A G and Shutko Y V 2011 *Appl. Phys. Lett.* **98** 021503
- [12] Zheng C, Shao T, Niu Z, Li C, Wang G, Tan J and Yan P 2011 *IEEE Trans. Plasma Sci.* **39** 2070
- [13] Shao T, Tarasenko V F, Zhang C, Lomaev M I, Sorokin D A, Yan P, Kozyrev A V and Baksht E Kh 2012 *J. Appl. Phys.* **111** 023304
- [14] Shao T, Zhang C, Niu Z, Yan P, Tarasenko V F, Baksht E Kh, Kostyrya I D and Shutko Y V 2011 *J. Appl. Phys.* **109** 083306
- [15] Shao T, Zhang C, Jiang H, Niu Z, Yan P and Zhou Y 2011 *IEEE Trans. Plasma Sci.* **39** 1881
- [16] Mesyats G A and Yalandin M I 2009 *IEEE Trans. Plasma Sci.* **37** 785
- [17] Yatom S, Vekselman V, Gleizer J Z and Krasik Ya E 2011 *J. Appl. Phys.* **109** 073312
- [18] Yatom S, Gleizer J Z, Levko D, Vekselman V, Gurovich V, Hupf E, Hadas Y and Krasik Ya E 2011 *Europhys. Lett.* **96** 65001
- [19] Yatom S, Vekselman V and Krasik Ya E 2012 *Phys. Plasmas* **19** 123507
- [20] Sorokin D A, Lomaev M I and Krivonogova K Yu 2010 *News Tomsk Polytech. Univ.* **316** 18
- [21] Yatom S, Stambulchik E, Vekselman V and Krasik Ya E 2013 *Phys. Rev. E* **88** 013107
- [22] Yatom S, Tskhai S and Krasik Ya E 2013 *Phys. Rev. Lett.* **111** 255001
- [23] Gigos M A and Cardenoso V 1996 *J. Phys. B: At. Mol. Opt. Phys.* **29** 4795
- [24] Bethe H A and Salpeter E E 2008 *Quantum Mechanics of One- and Two-Electron Atoms* (Mineola, NY: Dover)
- [25] Raizer Yu P 1997 *Gas Discharge Physics* (New York: Springer)